ORIGINAL PAPER

Hanging glacier avalanche (Raunthigad–Rishiganga) and debris flow disaster on 7 February 2021, Uttarakhand, India: a preliminary assessment

Renoj J. Thayyen[1] · P. K. Mishra[1] · Sanjay K. Jain[1] · John Mohd Wani[1] ·
Hemant Singh[1,2] · Mritunjay K. Singh[1,3] · Bankim Yadav[4]

Abstract

A catastrophic debris flow in the Rishiganga and Dhauliganga rivers in Uttarakhand, India, on 7 February 2021 left a trail of disaster. Around 100–150 people lost their lives according to Uttarakhand Chief Secretary statement given to ANI news portal, two hydropower projects were badly damaged and a bridge across the Rishiganga River was washed off in the event. Study shows that the debris flow is caused due to detachment of 0.59 km^2 right lobe of a hanging glacier and resultant ice-rock avalanche. This right lobe of the glacier was located over a mountain slope having an average slope of 35° at 4700–5555 m a.s.l. and travelled 12.4 km before hitting the infrastructure projects. Role of precipitation, snow cover, land surface temperature, and permafrost processes were investigated for identifying causes of the event. Since 2012, monsoon precipitation and mean annual land surface temperature (LST) showed significant increasing trend. Snow cover during monsoon months showed increasing trend and September, October and November experienced decreasing trend at glacier elevations. Mean annual LST increased from − 0.3 °C in 2012 to a peak of 0.4 °C in 2016. Central lobe of the glacier advanced during this period and eventually fell off in 2016 suggesting that the LST warming forced reduction of frictional drag at the interface facilitating it advancement and eventual dislodgement. Permafrost modelling suggests warm permafrost below 50 m and conditions favourable for intense frost cracking up to 10–15 m. At ~ 40 m depth, the delayed response of 2012–2016 warming produced peak positive temperature conditions by December and probably facilitated the formation of thin film of water at the deeper layers acting as a lubricant for glacier sliding. It is also suggested that the increase in summer precipitation might have forced thickening of the accumulation area and thereby increasing the shear stress for sliding of the glacier. It is proposed that the recent change in the weather conditions in the region is primarily responsible for this event through geological, glaciological, and permafrost processes. Flood modelling study suggests a flood volume of ~ 10 MCM generating 24.5 m flow depth at the bridge site with 12.7 m/s flow velocity. The event highlighted the need for improved monitoring of the cryosphere areas of the Himalaya to capture the early warning signs for better preparedness.

Extended author information available on the last page of the article

1 Introduction

A devastating flash flood occurred on Rishiganga and Dhauliganga rivers, which initiated from the upper glacier region of Raunthigad in the Chamoli District Uttarakhand. The event happened on 7 February 2021 and had a devastating effect downstream. Flood impact was mainly constrained to the infrastructure project along the river reach starting from a 13.2 MW small hydropower project across Rishiganga (2050 m a.s.l.) and then dismantling a bridge across the Rishiganga (1985 m a.s.l.) at the confluence of Dhauliganga. Further downstream at 4 km on Dhauliganga, the flood destroyed the 520 MW Tapovan-Vishnugad hydropower project (1800 m a.s.l.). The tunnel under construction for the Tapovan-Vishnugad project becomes the major disaster site, more than 77 people lost lives (Mehta et al. 2021) and 100–150 casualties reported (Asian News International 7 February 2021). Tapovan dam structure is filled with flood deposits highlighting the amount of debris brought down by the event. This debris flow in the peak winter month of February caused strong speculation about the cause of this event. This extreme event affects the landscape of the region and becomes more susceptible to landslide and debris flow events (Mehta et al. 2021). Considering that heavy snowfall occurred in the region a couple of days ahead, i.e. on 4 and 5 February 2021, an avalanche trigger is suspected as the Rishiganga basin has around 52 glaciers with a 262 km^2 glacier area. Five of these glaciers have an area > 50 km^2 (Sangewar et al. (2009), therefore, the possibility of a glacial lake outburst flood (GLOF) is also considered. However, a recent glacial lake inventory of the region prepared as part of an ongoing project under the National Mission for Sustaining the Himalayan Ecosystem (NMSHE) sponsored by the Department of Science and Technology, Govt. of India recorded 7 glacier lakes in the area with none of them is vulnerable as per standard criteria (Jain 2021, Under preparation). The high-resolution satellite images on the following day, 8 February (Source: Digital Globe https://www.maxar.com/open-data/uttarakhand-flooding/) given the first insight on the location of the flood initiation point in the Raunthigad catchment, a tributary of River Rishiganga. It has shown an avalanche site on the northern slopes at an elevation of 4700–6000 m a.s.l. Subsequent analysis of the previous day's images clearly showed that the avalanche occurred during the intervening period of 6th and 7th. This is followed by the availability of photographs taken during aerial reconnaissance survey conducted by various agencies, which clearly showed the source area of the avalanche (NTPC, personnel communication). By tracing back, the site information on google earth images and other satellite images showed that a "hanging glacier" was occupying the detachment area, which suggested that the event was initiated as ice–rock avalanche. The right lobe of the hanging glacier, which got detached, had a length of ~ 1.6 km and an average width of ~ 550 m (Mehta et al. 2021) occupied the northern slope in the Raunthigad catchment. This hanging glacier of 1.23 km^2 area situated at an elevation range of 4695–6000 m a.s.l. and detached right lobe had an area 0.59 km^2. This ice-rock avalanche resulted in massive debris flow with long-runout distance travelled through 14.35 km along Raunthigad to hit the hydropower project barrage (HEP-1) and washed off the bridge across River Rishiganga further downstream. About 7.4 km downstream, the debris flow devastated the Tapovan barrage. As the event occurred at forenoon

time around 11:00 AM, local residents could capture several live images and videos of the event illustrating the catastrophic dimensions of the floods (Fig. 1).

This is a very significant event not only in terms of the catastrophic disaster it caused along its flow path but also in terms of breaking of a large glacier mass which is a very rare phenomenon in the glaciated regions of the world and more so in the Himalayas. This event is followed by a previous catastrophic event in 2013 in the same region known as the "Kedarnath deluge". The 2013 event was caused by a combination of factors, including extreme rainfall, sudden snowmelt under excessive rainfall and breaching of Chorabari lake (Allen et al. 2016; Dobhal et al. 2013; Shukla et al. 2013) indicate the serious challenges faced by the mountain community in a warming climate. Hence, understanding the causes leading to this event is of utmost importance for assessing the disaster potential of the region in particular and also for the entire Himalayan region. Glacial lake outburst flood (GLOF) is well appreciated as a potent disaster of glacial origin, and a couple of recent events increased its threat perception in the region (Govindha Raj and Vinod Kumar 2012; Komori et al. 2012; Schmidt et al. 2020; Shukla et al. 2013; Thayyen 2020). Cloudburst is another disaster and its associated vulnerability that is increasingly becoming more regular in the Himalayan region (Das et al. 2006; Dimri et al. 2017; Kumar et al. 2018; Mishra et al. 2021; Mishra et al. 2022; Thayyen et al. 2013). Snow avalanche is also identified as a major disaster in the region, and forecasting and modelling are regular activities. But glacier avalanche is not considered as disaster component so far in the planning of infrastructure and development projects as well as regular activities in the higher Himalayan region.

In the mountainous glacial environments, the catastrophic mass flows are an essential geomorphic process that may pose a significant hazard to the infrastructure and the communities living downstream (Cuffey and Paterson 2010; Evans and Delaney 2015). These include a mass movement of glacial debris flows, ice-rock avalanches, and outburst-generated flows, occurring at a time when glaciers are shrinking in response to climate change (Evans et al. 2009; Evans and Delaney 2015). The 2002 event of Kolka glacier detachment

Fig. 1 **A** Pre-flood NTPC barrage (HEP 2) at Tapovan, **B** post-flood photograph showing severe damage to NTPC barrage at Tapovan, **C** site of washed off bridge across Rishiganga upstream of NTPC barrage, and **D** site of Rishiganga (HEP-1) project site. *Photograph courtesy: NTPC and BRO*
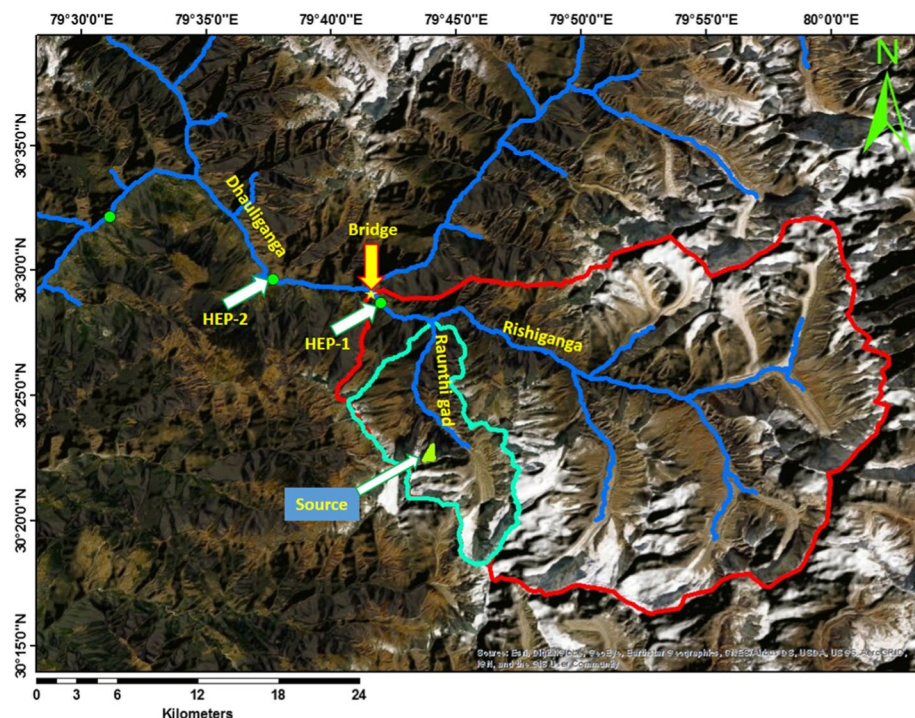
Fig. 2 The drainage map of the area showing the Raunthigad catchment and potential source area of the ice-rock avalanche, Rishiganga catchment and Dhauliganga and Alakananda rivers further downstream

in the Caucasus mountain, southern Russia, is a livid but rare example of such catastrophic events (Evans et al. 2009; Haeberli et al. 2004; Huggel et al. 2005). Closer home, the 5 May 2012 Seti River flood in Nepal initiated by the detachment of rock mass at the height of 6700 m a.s.l. from the south flank of Annapurna IV and ended up as colossal debris flow (Dwivedi and Neupane 2013; Hanisch et al. 2013; Kargel et al. 2014; Kim et al. 2017; OI et al. 2014).

Rockfall induced debris flow of Piz Cengalo, south-eastern Switzerland in 2017 (Mergili et al. 2020), the 2012 rock–snow avalanche in the Alps, Austria (Preh and Sausgruber 2015), and the 2012 multi-lake outburst flood in the Santa Cruz Valley (Mergili et al. 2018) illustrate the potent threat of such events in the cryospheric regions of world's mountains in a warming climate. In most of these events, the ambiguity remains regarding the accurate flow volumes involved and the mechanism of flow transformation, water source, etc. A detailed overview of these type of events could be found by Evans and Delaney (2015).

2 Study area

The ice-rock avalanche by detachment of the hanging glacier situated at headwater region of Raunthigad (Lat: 30°22′40.62"N, 79°43′57.66"E) in Chamoli District of Utta-rakhand (Fig. 2). Raunthigad originates from the Trishuli glacier, and the snout of the Trishuli glacier is around 1.5 km further ahead of the point where the ice-rock avalanche hit

the valley. The Raunthigad catchment has an area of 94 km^2 with a glacier cover of 16 km^2. Raunthigad catchment extends from 2380 m a.s.l. to 7120 m a.s.l. (Trishul peak) and joins with the Rishiganga basin. Rishiganga basin drains an area of 686 km^2 and has 52 glaciers with 177 km^2 glacier cover. For precipitation, snow, land surface temperature (LST) analysis, and assessment of soil thermal regime fluctuation, we drew an area of interest (AOI) of 3 km^2 around the hanging glacier on the northern slope. The geology of the area comprises of Jutogh, Almora formation and the area is close to Main Central Thrust (MCT) (Thakur 1992). Quartzite, marble and garnet, granite gneiss, etc. dominate this group.

3 Methodology

3.1 Area change of the hanging glacier

Glacier area change is estimated from 1985 to 2020 using satellite images and google earth images. Table 1 shows the satellite data description. Glacier boundary marked manually, and area change is calculated. The area of the hanging glacier in 1985 is also estimated from the Survey of India toposheet (53 N/11, 1: 50,000).

3.2 Glacier volume estimation

Glacier volume estimation is carried out using the standard glacier area–volume relationship:

$$V = \alpha A^y. \tag{1}$$

An average value of 1.36 has been arrived for the scaling index γ from depth-sounding (Bahr et al. 1997) and considered it as a global exponent. We used a volume estimate of the glaciers from the glacier inventory of the Geological Survey of India (GSI), which is based on the Muller's classification, to estimate the scaling constant as the scaling constant could vary from region to region. We found that for glaciers with less than 2 km^2 area, the average scaling constant is 0.024, and for bigger glaciers, 0.027 gives the best relationship between the variables (Thayyen et al. 2010). We used the following relationships to estimate the glacier volume in the present study for a range of possible glacier volume.

$$\text{Glaciers} < 2\text{km}^2, V = 0.024\ A^{1.36} \tag{2}$$

$$\text{Glaciers} > 2\text{km}^2, V = 0.027\ A^{1.36} \tag{3}$$

where V is the volume in km^3 and A is the area in km^2.

3.3 Land surface temperature of hanging glacier catchment Raunthigad catchment

Moderate Resolution Imaging Spectroradiometer (MODIS) Land Surface Temperature (LST) data was accessed from https://lpdaac.usgs.gov/tools/appeears/. All four daily data points of LST (MOD11A1) from Terra and Aqua satellites (~ 10:30 AM, 10:30 PM and ~ 01:30 PM and 01:30 AM) between 2002 and December 2020 (18 years) were downloaded. The batches were consolidated separately by clipping over the hanging glacier area of the Rishiganga basin. LST values in 4 grades with varying error

Table 1 Details of data products used in this study

Sl. no.	Data product name	Period of availability	Spatial resolution	File format	Remarks
1	Advanced Spaceborne Thermal Emission and Reflection Radiometer (ASTER) Global Digital Elevation Model	–	30 m	tiff	https://asterweb.jpl.nasa.gov/gdem.asp
2	High Mountain Asia 8-m Digital Elevation Models	–	8 m	tiff	http://dx.doi.org/10.5067/KXOVQ9L172S2
3	Sentinel-2	5 February 2021 (Pre-event); 10 February 2021 (Post-event)	10 m	tiff	https://sentinels.copernicus.eu/web/sentinel/home
4	Planet labs imageries (as screen shots from website)	3, 5 February 2021 – 09 February 2021	3 m; 5 m	.jpg	https://www.planet.com/
5	Digital globe	10 February 2021	0.5 m m	.jpg	https://www.maxar.com/open-data/uttarakhand-flooding
6	Google Earth Pro data	1985; 2003; 2005; 2012; 2015; 2017; 2019	15 cm–30 cm	.jpg	https://www.google.com/intl/en_in/earth/versions/

(error ≤ 1 K, ≤ 2 K, ≤ 3 K , and > 3 K) have been generated and built a continuous data series by incorporating the less accurate data in a hierarchical way (Yadav et al. 2020) n. The remaining gap is filled by interpolation. The satellite-derived LST data could vary significantly (Varade and Dikshit 2018) with the ground surface temperature (GST) data. To refine the LST data, we used 3 years (2016–2019) of rock temperature data generated in the Ladakh mountain range in western Himalaya (Fig. S1). Monthly regression equations were developed using the GST observation and MODIS LST for this site which provided a good match with observations ($R^2 = 0.92$, Fig. S1b). Using this monthly regression equation (Table S1), we generated the GST equivalent of LST for the avalanche area for further modelling of ground temperature regime using the GEOtop model (Endrizzi et al. 2014).

3.4 Precipitation over hanging glacier catchment and nearby stations

Precipitation changes in the region are analysed by using the station observation from Chamoli (30.293 N, 79.56E) since 2000 and GPM IMERG Final Precipitation L3 1 day 0.1 degree $\times$ 0.1 degree V06 (GPM_3IMERGDF) (Huffman et al. 2020) (available at https://disc.gsfc.nasa.gov/). The daily files from the datasets were clipped to the ice-rock avalanche site in the Raunthi catchment.

3.5 Snow cover change over the hanging glacier area

Accurate snow cover assessment in the monsoon-dominated regions of the Himalaya is a challenge due to persistent snow cover (Awasthi and Varade 2021). A new methodology proposed by Singh et al. (2019) is used to generate the elevation-depended snow cover change since 2000. For generating daily Snow cover area (SCA), MODIS daily Snow cover products, e.g. MOD10A1 and MYD10A1 version 6 (V6) from Terra and Aqua were downloaded from the NASA earth data website (https://search.earthdata.nasa.gov) and re-projected into UTM WGS84 projection. All the initial classes of the downloaded products are reclassified into three major classes (0 = cloud, 1 = non-snow, and 2 = snow) as defined in Table S1.

ALOS World 3D, distributed freely by the Japan Aerospace Exploration Agency (JAXA) is downloaded to the same extent as MODIS SCPs from the open topography website (https://portal.opentopography.org/dataCatalog?group=global). Downloaded ALOS Word 3D DEM is resampled and re-projected using bilinear interpolation to have the MODIS SCPs projection and spatial resolution. This resampled DEM is then used for the generating slope direction (Aspect) and elevation zone map. Aspect map is classified into four distinct directional classes (North-east, South-east, South-west, and North-west). DEM is classified into 10 zones with a range starting from < 2000 m as 1st zone, after that, subsequent zones are of 500 m elevation interval up to 6000 m elevation. Elevation of More than 6000 m is classified as 10th zone. Sub-watershed data is generated from the same DEM using open source hydrological analysis tools. After generating all these files, daily cloud-free SCPs are generated by processing MODIS SCPs using the methodology proposed by Singh et al. (2019). The methodology proposed by Singh et al. (2019) consists 5 successive logical steps consisting of Temporal filtering, Combining Terra and Aqua SCPs, Aspect-wise mean Snowline, and No-Snow line altitude conditioning for sub-watershed and elevation-based moving filter. Temporal filtering is employed for the same period as suggested by Singh et al. (2019) for Himalayan terrain. After completing all the steps,

cloud-free SCPs received from the fifth step are clipped using the study area boundary and further used to generate elevation zone-wise daily SCA (in %) statistics.

3.6 Modelling of soil thermal regime

For the past two decades, the soil temperature at the study site was simulated using the GEOtop (Endrizzi et al. 2014). Only the soil part of the model was used with water transport disabled. The model was run in a one-dimensional model with a Dirichlet boundary condition at the top and a Neumann boundary condition at the bottom. The MODIS land surface temperature was used at the top, and flux of 0.0 W m^{-2} was used at the lower boundary. The simulation of soil temperature is carried out for high diffusivity conditions with a heat capacity equal to 2.25×10^6 J m^{-3} K^{-1} and the thermal conductivity equal to 4.0 W m^{-1} K^{-1}. Due to the non-availability of parameters, the model parameters typical to granite rocks available in the literature were used (Gubler et al. 2013). The depth of the modelling soil column was kept up to 100 m and was initialised with an initial temperature of -2 °C. Before analysis, the model was run 50 times to attain thermal equilibrium (Pogliotti 2011; Wani et al. 2020). Further details about the experimental design could be found in Wani et al. (2020).

3.7 Flood modelling

The design flood hydrograph of the flood event was generated using Soil Conservation Service (SCS) dimensionless unit hydrograph (DUH) methodology (Jeng 2006; Service 2007; Thayyen et al. 2013), now Natural Resources Conservation Service (NRCS) developed a DUH based on the analysis of many watersheds. It approximates the flow from an intense storm from a small watershed. The SCS hydrograph arbitrarily has 100 units of flow for the peak and 100 units of time for the duration of flow. The SCS DUH consists of 37.5% of the total runoff volume before the peak discharge and the remaining volume after the peak discharge occurs. The total base of the DUH is 5 times the time to peak (T_p). It has 19 constant ordinates that represent percentages of flow and time. The DUH is scaled to various size storms events using three conversion factors. To develop the design hydrograph, we required the likely total runoff volume, storm duration, and stream dimension.

We also attempted one-dimensional unsteady flow hydraulic modelling using HEC-RAS 5.0.7 using the design hydrograph discussed above up to the NTPC site located at Tapovan to understand the flow velocity and flow depth.

The freely available digital data of Advanced Spaceborne Thermal Emission and Reflection Radiometer (ASTER) Global Digital Elevation Model of 30 m resolution is used to delineate Rishiganga and Raunthigad watersheds, generation of elevation profiles, drainage lines, x-sections, and other hydrodynamic parameters. Multi-date remote sensing data of Sentinel-2 for pre-event and post-event were used to assess the extent of damage due to the event. Sentinel-2 has 10 m ground resolution and twelve spectral bands of a different wavelength. One scene for each of the pre-event (6–7 February 2021) and post-event (8–9 February 2021) of the avalanche initiation area was used for the analysis. We have cross-validated the results using the fine-resolution data (3 m × 3 m) shared by the Planet lab. Further, open data 0.5 m spatial resolution from digital globe (https://www.maxar.com/open-data/uttarakhand-flooding) for 10 Feb., 2021 was used for analysing the post-disaster stream morphology changes from the source area to 23.58 km till HEP-2 site at Tapovan.

4 Results and discussion

4.1 Area change of the hanging glacier and early indicators

Like any other glacier, a hanging glacier is a dynamic ice mass with internal flow and deformation in response to the climate forcing and mass balance regime. As glaciers move under gravity, the mountain slope on which it sits become a critical factor. As per the survey of India (SOI) toposheet of 1984, this hanging glacier had an area of 1.7 km² which reduced to 1.23 km² in 2017. The glacier has right, centre and left lobes in which most of the change during these 33 years was recorded at central and left lobes, with the right lobe remaining at its place. This suggests that the right lobe was in the steady-state condition during this period (Fig. 3) with a flat glacier tongue which flows from 5555 m a.s.l. to 4700 m. The glacier occupied a mountain slope having an average slope of 35°. The headwall above the bergschrund has a higher slope of 49°. The central part extended from 5788 m a.s.l. to 5500 m at lower margins, and the left lobe extending from 6040 to 5180 m a.s.l. The most visible signs of the climate forcing on a glacier are its area change over a period. From 1984 to 2003, the glacier area reduced to 1.38 km² from 1.7 km² (Fig. 3).

From 2005 the glacier experienced further area loss to 1.27 km². However, by 2012 central glacier lobe advanced by around 236 m and recorded a corresponding increase in area to 1.3 km². The advancement of the central lobe continued during 2013, 2014, and 2015 reached 1.351 km² in 2015. Overall advancement of the central part of the glacier from 2005 to 2015 was around 330 m. This central part of the glacier was sitting over
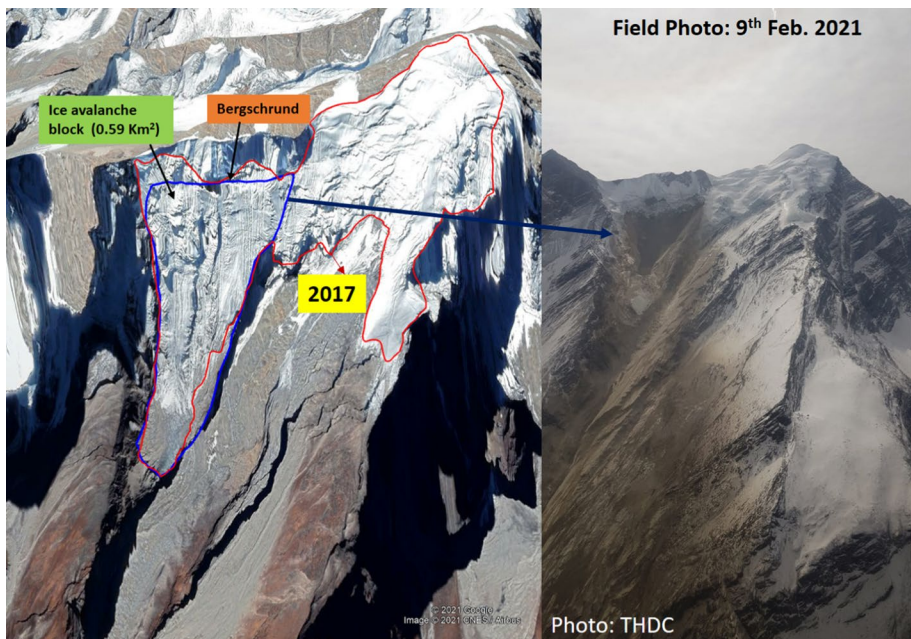

Fig. 3 A Hanging glacier in google earth image of 2017. The detached right lobe is marked blue. **B** Heli photograph of 9 February 2021 of the site showing detachment of the glacier creating an ice-rock avalanche. (Photograph courtesy, THDC)

the steep and plain bedrock. A close look at the surface conditions of the glacier shows a certain degradation of the glacier at "C" area with the development of multiple cracks in 2012 and 2015 images (Fig. S2). It suggests that the glacier has either moved from the quiescent phase to the active phase during the period (Röthlisberger 1987) or advanced due to enhanced accumulation. Between 2016 and 2017, all the glacier area which showed advancement till 2015 has got detached, and the glacier area reduced to 1.23 km², recording an area loss of 0.121 km² and remain more or less same way till 2020 with little shrinkage of the central part. This analysis suggests that the central lobe of the glacier was continuously under recession during the last 3 decades with surge like advancement and sudden degradation. The right lobe, which remained in its position through these 33 years, got detached on 7 February 2021 and caused the catastrophic flood. Figure 3 shows the detached part of the hanging glacier and a post-event field photograph showing its geometry. This shows that the glacier is detached from the bergschrund (Mehta et al. 2021) and the sharp edges of the crown suggest that the glacier was not sliding at its bed which is also indicated by the steady positioning of the right lobe for the past 33 years. The detachment of the central lobe in 2016 seems to indicate the vulnerable conditions of this glacier.

4.2 Glacier volume estimation and other water sources for debris flow

The total area of the Hanging Glacier in 2019 was 1.23 km², and the area of right lobe of the glacier, which fell off on 7th in 2019, was estimated to be 0.59 km² (48%). Using the area–volume scaling, the volume of the detached part of the glacier is estimated to be in the range of 11.7 to 13.2×10^6 m³. Snow over the glacier is not accounted for this estimation. Since there was heavy snowfall in the 2019 winter and two days before the event in 2021, it is suspected that significant snow accumulation happened over the glacier. The surface features of the hanging glacier prior to the avalanche in the satellite image of 5 December 2020 show thick snow accumulation over the glacier (Fig. S3). The volume of water in the debris flow could be higher as about 14 km runout stretch of the avalanche, till it joins Rishiganga River was snow-covered and could be incorporated in the debris flow matrix. Another source of water is the soil moisture as reported in the events reported earlier from other parts of the world by entrainment of large quantity of soil and rock (Evans and Ge 2017), eventually turning it into a debris flow and facilitating melting of the huge glacier ice mass with frictional heat generated during it high velocity down slope movement. This particular aspect needed detailed study and not attempted in this preliminary assessment.

4.3 Ridge and valley slope profile

Figure 4 shows the elevation profile drawn from the ridge top of the Raunthi glacier area to the HEP 2 at Tapovan, traversing a distance of 23.58 km. Above the bergschrund, a 138 m section with a steep mean slope of 49° connects to the ridge at 5688 m a.s.l. On the left, the glacier flows down from Raunthi peak at 6063 m a.s.l. The right lobe of the glacier is 1.6 km long and with a mean slope of 35 degrees with its terminus at 4700 m a.s.l. The avalanche travelled a distance of 1.95 km through bedrock with a mean slope of 33° before striking the valley floor 3834 m a.s.l. The ice-rock avalanche converted into a debris flow during its transport through the valley with 7° mean slope for another 12.4 km till HEP 1. Between the bridge site and HEP 2, the average channel slope was 5.6°.
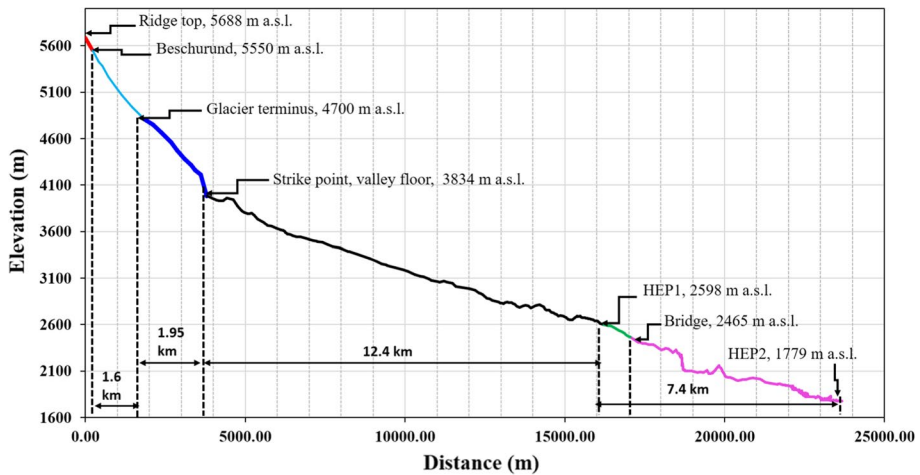
Fig. 4 Elevation profile for the stretch between ridge top to HEP 2 at Tapovan

4.4 Precipitation over hanging glacier catchment and Raunthigad

Precipitation and forms of precipitation, liquid or solid, is critical for glacier behaviour and thermal regime of surrounding periglacial areas. The southern slopes of the Himalaya are highly influenced by the monsoon precipitation and show elevation and topographic dependencies (Bookhagen et al. 2006, 2010). As this glacier occupied an elevation of 4695–5550 m a.s.l. It is expected that monsoon precipitation can occur as rain or snow or as a mixture depending on the prevailing atmospheric conditions. The Raunthigad catchment, where the glacier is situated, forms the northern boundary of the monsoon influence zone of the southern slopes (Fig. 5), and the topographic control (TC) (Yadav et al. 2020) runs through the northern ridges of Raunthigad reaching up to 7120 m a.s.l. (Trishul peak). This is a critical factor as monsoon-dominated areas of Uttarakhand Himalaya have less than 20% glaciers compared to the monsoon deficit zone in the north of the TC, suggesting less favourable conditions of southern slopes for glaciers. This also demonstrated by shallower temperature lapse rates at the monsoon-dominated glacier areas suggesting a high energy system through latent heat release of precipitating monsoon (Thayyen et al. 2005; Thayyen and Dimri 2018; Yadav et al. 2020). Nearest high elevation precipitation station located at Chamoli (2640 m a.s.l.) experiences annual precipitation in the range of 2659 mm to 850.8 mm. Monsoon precipitation in July and August constituted 53% of annual precipitation during the 2000–2009 period, which increased to 65% 2010–2017 period. Annual precipitation shows an increasing trend with a steep increase since 2010 (Fig. 6a). Most of this increase is attributed to July, August precipitation (Fig. 6b). Satellite-derived precipitation data (GPM) of 2001–2019 for the Raunthigad ice-rock avalanche grid show annual precipitation of 1352 mm with 998 mm w.e. (74%) precipitation occurring in summer months (May to October) and average 354 mm w.e. in during winter period. Annual precipitation derived from GPM for glacier area also shows a nominal increasing trend as well as for monsoon months of July, August as experienced at Chamoli station (Fig. 6). Both the data set suggests an increase in monsoonal precipitation in the region, especially since 2010. GPM data also suggests 2019 experienced the heaviest winter
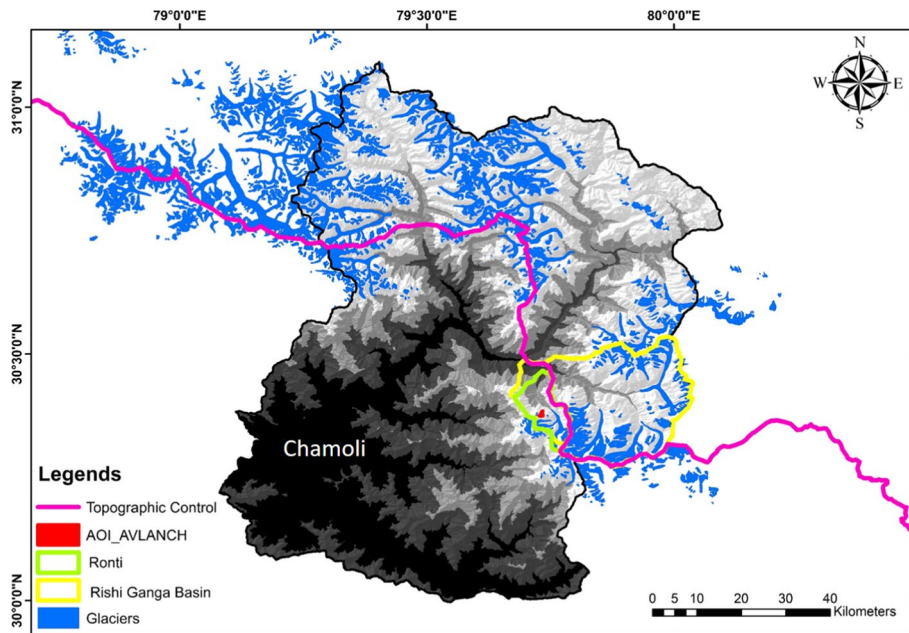
Fig. 5 Topography control (TC) dividing the monsoon and monsoon deficit zone in Uttarakhand. Note the location of the Raunthigad catchment and the location of the avalanche zone southern side close to the TC (Yadav et al. 2020)
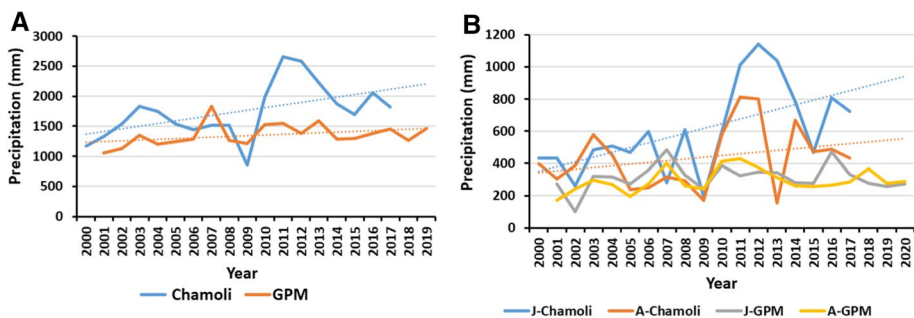

Fig. 6 Precipitation over the region showing an increasing trend for the station and GPM data: **A** annual precipitation and **B** July and August precipitation

precipitation since 2001 with 577.7 mm w.e. of snowfall which is corroborated by snow cover assessment of the region (Singh et al. 2019).

4.5 Snow cover change over the hanging glacier area

Change in the snow cover characteristics is a critical aspect that alters the temperature regime of high elevation non-glaciated land surface and dynamics of glaciers through mass balance. Elevation-depended snow cover variations were observed in the nearby Bhagirathi

basin from 2000 to 2019 period showing declining snow cover trend in December between 3000 and 6000 m a.s.l. elevations and an increasing trend in June for 4500–6000 m a.s.l. elevations (Singh et al. 2019). Snow cover variation is assessed over the hanging glacier area and elevations as well as for the Raunthigad catchment using the modified cloud removal algorithm (Singh et al. 2019). The study shows an increasing snow cover trend in July and August for elevation band 4000-5500 m a.s.l. and a declining trend in snow cover in September to November months for elevation between 4500 and 6000 m a.s.l. (Fig. 7), especially after 2010. The increase in snow cover is in tandem with the increase in precipitation observed above, and decrease in snow cover during September, October, and November in also match with the increase in LST observed during these months (Sect. 4.6). Summer snowfall in lower elevations is always a mix of rain and snow and does not sustain over a warm land surface in summer for a longer duration. Daily snow cover assessment shows short duration snow cover during these summer months. The declining snow cover trend of September to November supports this observation. However, summer snow on the glacier surface could stay longer, depending on the rain–snow ratio in the precipitation and could impact the glacier mass balance positively. The declining trend in snow cover during pre-winter months and increasing trend in summer monsoon months become highly significant after 2010.

4.6 Land surface temperature of hanging glacier catchment Raunthigad catchment

Land surface temperature (LST) of 3 km^2 area around the hanging glacier, most of it covered by exposed bedrock, is studied for evaluating the site-specific LST changes. The southern slope of the ridge is fully exposed in summer, and the permanent snow and ice are restricted to the northern slopes close to the ridge elevations. Mean annual LST during 2001–2020 range between −0.3 and 0.4 °C period and show a steady rise from low LST of −0.3 °C in 2012 to 0.4 °C in 2016 (Fig. 8a). July and August months recorded a maximum LST of 11.5 °C and a minimum of −11.7 in January. LST of July shows an insignificant negative trend, and August shows no specific trend. LST of September and October represent temperature regime at the end of the water year, which also shows a significant
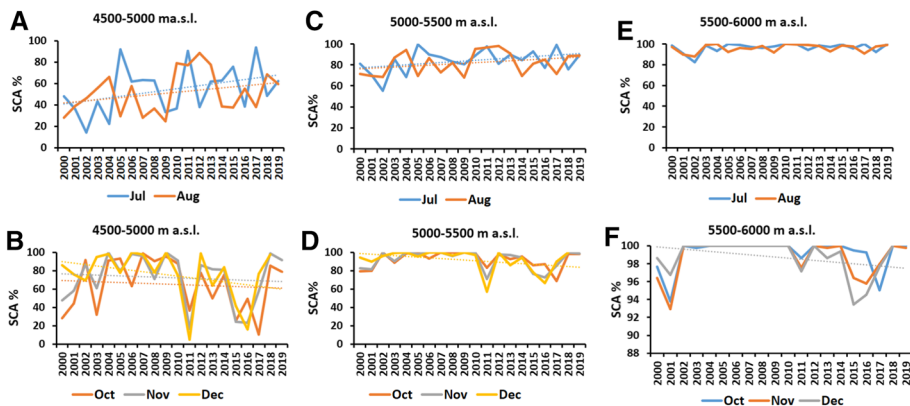

Fig. 7 Elevation-depended seasonal change in snow cover in the glacier elevations of Raunthigad showing an increasing trend in monsoon months and decreasing trend in October, November, and December months. Decreasing trend is significant since 2010
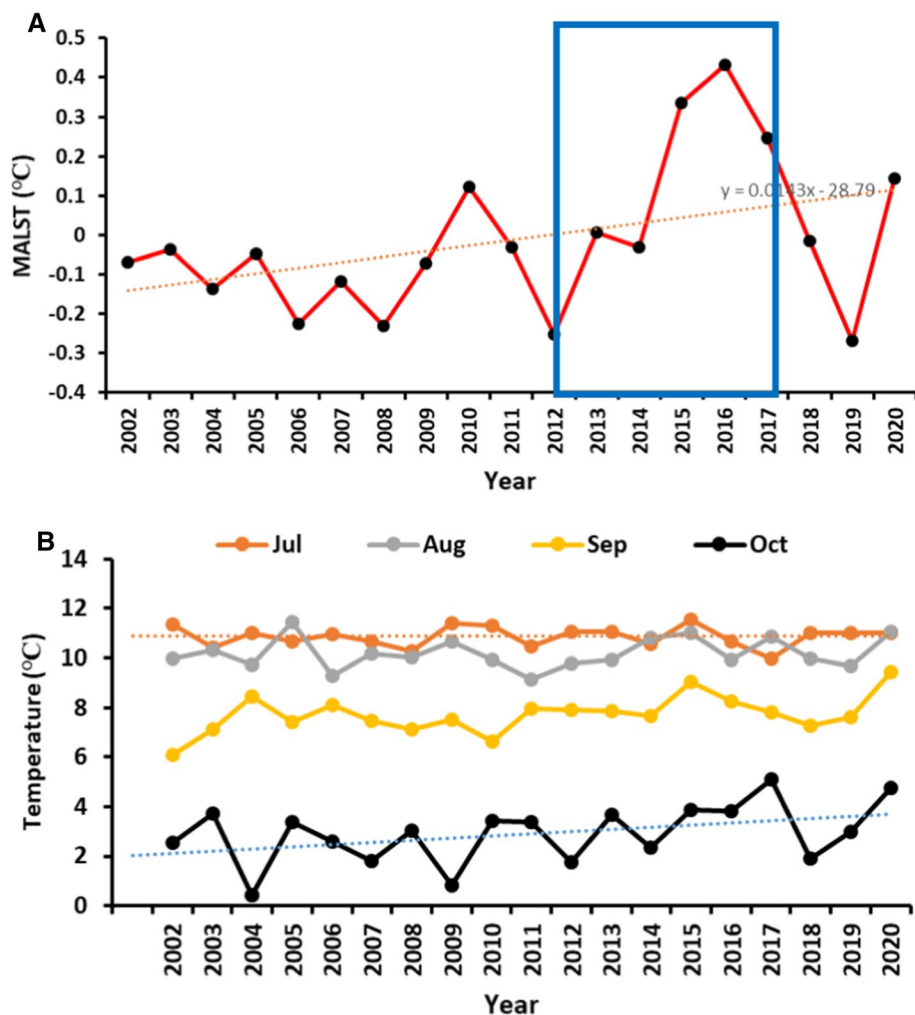
Fig. 8 A Mean annual LST variation around hanging glacier area during 2002–2020 and **B** LST variation during July, August, September and October showing a significant rise from 2012 to 2016 also reflected in October LST. Peak monsoon months show no increase in LST

rise from −1.9 °C in 2009 and 9.1 °C in 2017 (Fig. 8b). LST increase in September and October months (Rana et al. 2021) is mainly attributable to the reduced snow cover in these months. This clearly indicates warmer surface conditions build up around the hanging glacier area since 2012, facilitating the basal ice melt around the margins of the hanging glacier, especially at the lowermost zone, which seems to be firmly coupled with the bedrock earlier. This can also explain the surge like advancement of around 330 m noticed in 2015 as basal melting due to warmer temperature reduces the basal resistance and further warmed up the glacier ice, which facilitated the enhanced flow of the central lobe of the glacier (Part D in Fig. S1). This advanced section got removed during the 2016–2017 period suggesting this section probably detached and fell as a block rather than melting away. Considering the LST warming since 2012, this could be considered as a precursor

to the present event. The rock exposure caused by this event probably helped further the warming of the glacier frontal area.

4.7 Ground thermal regime variation

The response of small glaciers and ice aprons situated over the bedrock on the mountain slope is impacted by surface accumulation and the thermal regime of the bedrock. Bedrock warming could lead to basal melting and eventual decoupling of the glacier from the bed. As this glacier is situated in the elevation band of 4695–6000 m a.s.l, the possibility of the existence of permafrost areas and its thawing under a warming climate also could lead to slope failures. Recent studies in the Ladakh Reference Himalaya suggests permafrost condition above 4900 m a.s.l. Hence, a preliminary attempt is made to assess the soil thermal regime of the area surrounding the hanging glacier. In the absence of any ground-based temperature data from the region, daily refined LST regressed to the ground surface temperature of the 2002–2020 period and used to model the soil thermal regime up to 100 m. The thermal envelop curve for 20 years under high diffusivity condition suggests that the area has warm permafrost below 50 m with mean annual rock temperature at 50 m range between -0.0021 and -0.0031 °C (Fig. S4). The warm permafrost that is defined as permafrost with temperature at or higher than -1.0 °C (Changwei et al. 2015; Cheng and Wu 2007; Wu and Zhang 2008). At 40 m, this range changes to 0.0061 to -0.0006 °C suggesting non-permafrost conditions. However, using low diffusivity values, the region shows permafrost condition at a depth of 10 m with an annual temperature range of -0.074 to -0.126 °C. The site photographs suggest that rock mass detachment occurred from deeper zones. The standard values of rock parameters for granite match with the high diffusivity condition. Hence we considered only high diffusivity values for further analysis. The modelled daily temperature variations at 10, 15, and 20 m depths show seasonal temperature variations suggesting the conducive seasonal thermal variation for frost cracking up to 10–15 m depth (Fig. 9a). Figure 9b shows low amplitude seasonal variations in temperature at 20 m. This is due to a sustained sub-zero mean annual surface temperature which converted to high amplitude seasonal fluctuations once the surface temperature becomes positive and rising since 2012. At 40 m, this variation reflected as sustained sub-zero (-0.0001 to -0.0006 °C) from 2011 to 2018 period and moved to the positive regime from 2019 to 2020 up to 0.0052 °C. The delayed response of rising surface temperature at the deeper layers is clearly illustrated in Fig. 10. At 40 m, the response of temperature increase (2012–2016) reached after a 4-year delay. This shifts between freezing and thawing regime at this depth under warm permafrost conditions probably made this depth more vulnerable for detachment. As discussed earlier, below 50 m depth permafrost conditions prevailed during the past 20 years, and depth between 40 and 50 m provided favourable conditions for the present detachment forced by warmer weather conditions since 2012 suggesting clear signals of climate forcing on the present event (Fig. S5).

As the glacier is placed over the bedrock, significant seasonal variations in temperature regime are observed, with rock surface temperature rising to 18 °C in the summer months. The month of October showed a higher rate of warming (Fig. 8a). This high temperature of the rock mass surrounding the hanging glacier melts the glacier margins and helps it decoupling from the bed. At 10 m, also peak annual temperature is the range 0.6 to 0.8 °C and susceptible to melting under prevailing conditions. The surface warming is particularly sharp in October (Fig. 8b Oct.), especially during the 2009–2017 period when October LST shows a sharp increase from 0.8 to 5.1 °C.
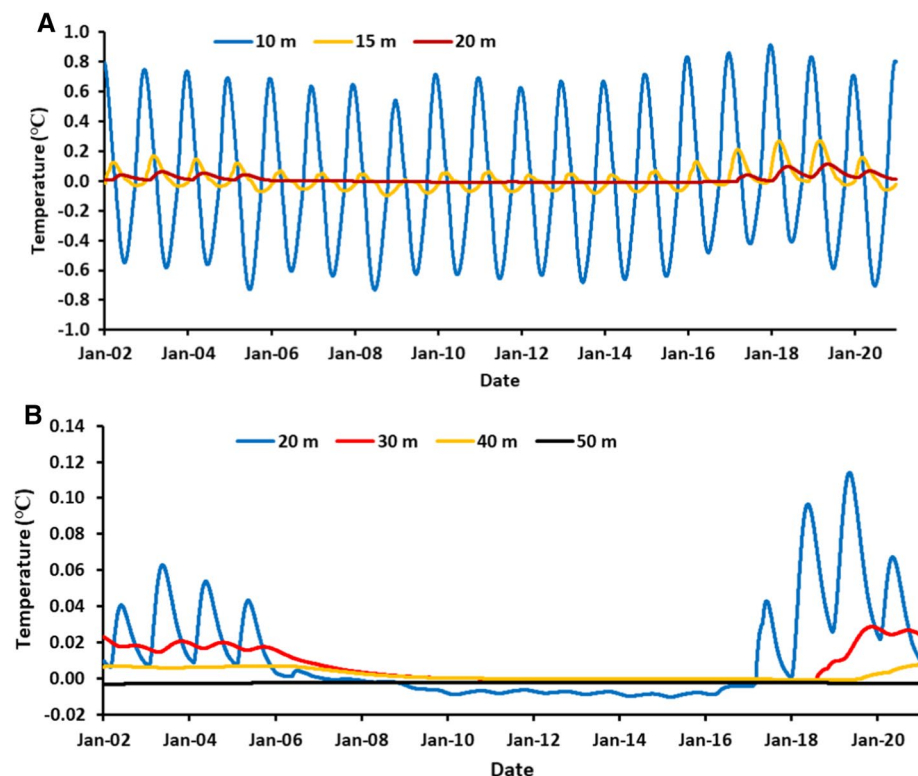
Fig. 9 **A** Modelled monthly mean temperature variation at **A** 10,15 and 20 m and **B** 20, 30, 40, and 50 m showing the seasonal changes and delayed warming towards deeper depths
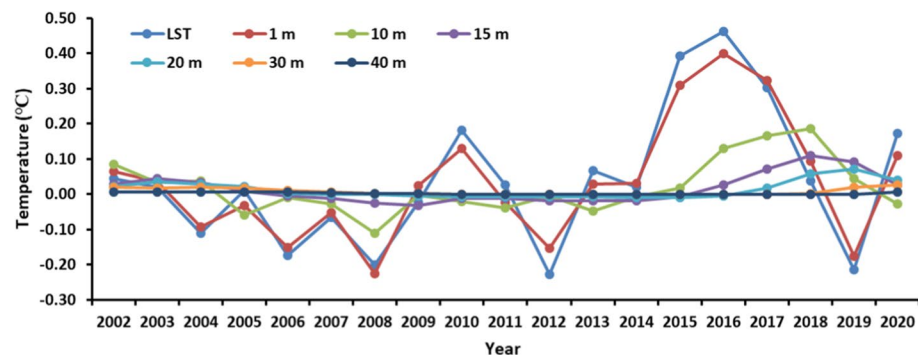

Fig. 10 Delayed response of deeper depth to LST increase from 2012, which peaked in 2016. A 4-year delay at 40 m forced the highest temperature between 40 and 50 m during December–February

Refreezing of this meltwater further melts the basal ice by the latent heat release. Recurrence of this process over 10 or more years could have widened the rock fissures and reduced basal adhesion. For thick temperate glaciers, a thin film of water at the basal zone is very normal, maintained by the pressure melting even in winter months. At 40 m and

below it is observed that an incremental increase in the temperature during the 2002–2020 period and a sharp increase in temperature at 40 m depth from sub-zero to 0.008 °C (Fig. S5). This could be a factor that facilitated this event happening in February. It is possible that the depth assessment of active layer may vary as we used LST proxy in place GST.

5 Discussion

Considering the deep scar with unknown depth associated with the hanging glacier's right lobe, which detached on 7 February 2021, it could be a case related to the sudden movement of the hanging glacier linked to basal sliding. Glacier ice thickness and surface slope (α) are the two important parameters determining the basal shear stress (τ_b),

$$\tau_b = \rho g h \sin \alpha \tag{4}$$

where ρ is glacier ice density, g is the gravitational acceleration. In general, glacier flow constitutes differential movement within the ice by internal deformation and sliding of the glacier on its bed illustrated by the following equation by Paterson (1994):

$$u = Ah^{n+1} \sin^n \alpha + Bh^m \sin^m \alpha \tag{5}$$

u is velocity under non-steady flow conditions, h is ice thickness, α is glacier surface slope, and A, B, m and n are constants. The first term represents the differential movement within the ice, and the second represents the basal sliding. The well-defined geometry of the scar suggests that the glacier was firmly frozen to its bed with boulder entrainment so far without any basal sliding. The apparent stability of this particular section that fell off had a well-defined ablation tongue that flowed down to the lower elevation (4695 m a.s.l.) compared to the central lobe of the frontal glacier region (5500 m a.s.l.). In the case of basal ice containing rock debris, the effective basal shear stress is $\tau_b = \tau - \tau_f$, where τ_f is the frictional drag stress counteracting the shear stress (Paterson 1994). In the present case, it could be the case of $\tau_b < \tau_f$ prior to this event that held the glacier firmly in its place so far. The basal drag stress is formulated as (Paterson 1994),:

$$\tau_f = \mu B C \eta \hat{w} \tag{6}$$

where μ is the coefficient of rock–rock friction, C is the debris concentration, B is a parameter with dimension m^{-1} describing the characteristic of the bed, η is effective viscosity of ice and $\hat{w}$ is the average component of ice velocity perpendicular to the mean bed. Survey of India toposheet, 1984 mapped this glacier covering 1.7 km^2 of area, While the central and left lobes receded significantly during 1985–2017 (Fig. 11). The left lobe, which detached, showed no recession or advancement, suggesting that this section probably remained under steady-state flow conditions during the period. Thus the equilibrium condition is governed by Paterson (1994):

$$-\rho g h \frac{dh}{dx} \delta x + (\rho g h \sin \beta) \delta x - \tau_b \delta x = 0. \tag{7}$$

This condition facilitates "over deepening" especially if the glacier occupies bedrock with a steep slope and provides vulnerable zones under prevailing geology. The Main Central Thrust (MCT) run close to the Raunthi catchment and is tectonically highly active
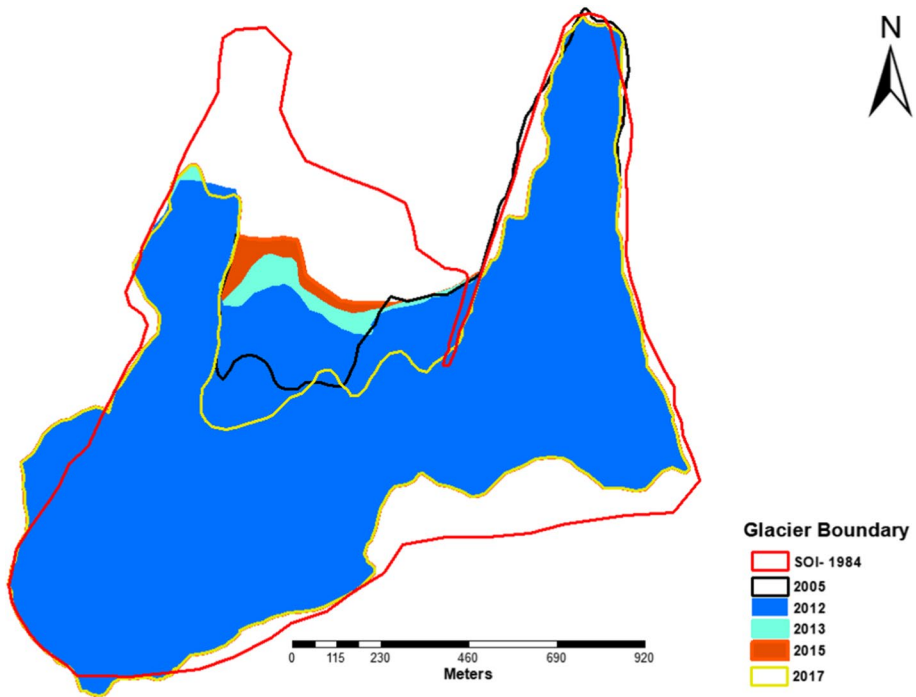
Fig. 11 Glacier area change since 1984 showing steady-state conditions of right detached lobe for 33 years and significant area change for left central lobes

under the zone-5 category. Hence, for the last more than hundred years, glacial processes over this fragile zone might have facilitated significant over deepening under this glacier. The over deepening of the glacier bed occurs as shear stress at the bed is determined by the surface slope. Ice flow is in the direction of maximum surface slope, even if the bed slope is in the opposite direction (Paterson 1994), if such a situation exists due to local geological factors. The over deepening occurs most where maximum ice flow occurs and that usually happens at the equilibrium altitude (ELA) for small glacier with a steep slope.

It is observed in some instances that the product of erosion can build up at the glacier bed, and lips of cirque and over deepening are coated in sediments (Alley et al. 1999; HOOKE 1991). The erosional process at the glacier bed is modelled by MacGregor et al. (2009) as below:

$$\dot{\varepsilon} = \left(C_3 \times \psi_{\text{sed}} \times u_{\text{slide}}^2\right) + \left(C_4 \times u_{\text{slide}} \times \sin \beta\right) - \left(C_5 \times (\tan \alpha / (2 \times \tan \beta))\right). \qquad (8)$$

The first term represents abrasion, the middle term represents quarrying, and the third term represents negative feedback on quarrying based on local thickness of sediment (till). In the present situation, abrasion was not probably taking place as sliding of the glacier over long period of time is the pre-condition for significant abrasive erosion. Here, plucking or quarrying is the dominant process where the over deepening process already provided significant rock mass attached to the glacier body, and any situation facilitating or initiating glacier sliding can move the material. Quarrying is a function of slope, and sliding velocity (MacGregor et al. 2009) and the steep slope of the present glacier is a facilitating factor

for the process. These are long-term glacial processes under which glacial landforms are formed and well established in the glaciology literature. Here, the changes in the regional climate as we observed during the past 20 years probably played a critical role in facilitating the sliding of the glacier leading to the ice-rock avalanche due to glacier detachment.

5.1 Role of recent changes in the regional climate

Recent warming at the high elevation region seems to have resulted in the differential response at two closely placed elevations. Increased precipitation in summer monsoon months of July and August as evident from the precipitation data is one of the critical factors. Part of this increased precipitation falls as snow, as evident from the snow cover assessment as glacier elevations show an increase in snow cover during July and August. This monsoon snow over the non-glacier area melts away faster in a warm ground thermal condition as July and August LST range between 12 and 17.9 °C. This situation leads to an observed decreasing trend in snow cover in September, October, and November (SON) months and a corresponding increasing trend of LST in October. The impact of reducing snow cover in the region is also reflected in the cancellation of the Auli (a nearby ski slope) winter games in 2012, 2013, 2015, and 2016 (https://bit.ly/38MfFgz). The snow that falls over the glacier, especially in the higher elevation, reduces the glacier melt and eventually increases the glacier thickness in the accumulation zone, forcing incremental shear stress over the glacier and at the glacier bed, facilitating faster movement. On the other hand, increasing ground thermal regime due to regional warming, reduction in snow cover and exposure of more bedrock area due to glacier wastage all facilitate increased basal melting, especially at the glacier margins leading to reduce the basal adhesion facilitating the glacier sliding. Permafrost identified in the area also played a crucial role in facilitating the ice–rock avalanche. Changing active layer dynamics of the permafrost under warm land surface conditions could enhance the frost cracking of the bedrock fissures. Additional water from enhanced monsoon precipitation over the region might have exacerbated these processes by providing more water to the system. Annual freezing and thawing of the ~ 40 m active layer under warmer and wet conditions probably exacerbated the weakening of the basal adhesion. In some situations, frost cracking is found to be most active under a mean annual ground surface temperature (MAGST) between $+4$ °C and -7 °C (Savi et al. 2021). In the present case, the LST proxy of MAGST ranges between -0.3 and 0.4 °C and remains within the zone of active frost cracking.

The effect of the enhanced ground thermal regime since 2010 is evident and visible at the glacier zones where the glacier is not anchored over the bedrock as seen in the advancement of the central lobe of the glacier sitting over the plain bedrock surface in 2012 with reference to its 2005 position. Development of thin film of basal water due to warming of the ground thermal regime as showed earlier could change the bed characteristics, B (Eq. 6) and lubricate the ice-bedrock interface and reduce the rock–rock friction, μ allowing the basal slip to happen. Hence, an increasing trend in the mean annual LST, especially from 2008 to 2016, from -0.2 °C to 0.4 °C could be a critical factor as it further translated into the warming of ground thermal regime and associated basal and glacier margin melting. This is clearly visible in the advancement of the central lobe of the glacier (2012–2015) facilitated basal sliding without any significant basal drag due to basal melting because of warming bedrock coinciding with the LST warming. This resulted in an advancement of 220 m between 2005 and 2012, which increased to 264 m in 2013 and 320 m in 2015, and eventually the detachment

of about 435 m long section between 2015 and 2017 (Fig. 11). Bedrock slope in the range 33° probably assisted this process. Around 0.121 km^2 of the central lobe got detached probably in 2016 associated with the highest mean annual LST recorded since 2002. Modelling results show (Fig. 10) that the 2016 LST peak propagated down and resulted into increase in thermal regime at 40 m with a lag of four years. Hence, we think both these events are closely linked to the 2016 peak temperature preceded by the warming taking place since 2012. Therefore, this detachment in 2016 was a clear warning sign of the deteriorating health of the cryospheric system which culminated in the present disaster.

When recently exposed, bedrock undergoes sudden seasonal temperature variations leading to higher thermal stress, which may increase its susceptibility to rock break down (Fischer et al. 2006; Huggel et al. 2012; Wegmann et al. 1998). Under these facilitating conditions, 2019 experienced the heaviest snowfall in the last 20 years (Singh et al. 2019), which could have accumulated a significant amount of snow over the glacier. Further, heavy snowfall on 4 and 5 February 2021 (Rana et al. 2021) also added more amount of snow over the glacier. The image just a day before the event shows thick snow accumulation over the glacier, especially above the bergschrund. Such thick snow over the non-glaciated region leads to an eventual warmer ground condition in the winter months compared to snow-free conditions due to the insulation character of the snow. This reflects a lower freezing index of GST during high snow condition as compared to low snow condition Therefore, the seasonal snow accumulation preceding the event might have provided a warmer condition around the frontal margins of the glacier. On the other hand, deeper layers of bedrock up to ~ 40 m were warming as a result of delayed response to LST increase recorded between 2012 and 2017. Figure 10 shows the lag associated with thermal regime change between the top and bottom layers of the bedrock. The increase in soil temperature of 40–50 m depth initiated in 2012 show highest values in December 2020 (probably persisted through February 2021), probably producing conducing warm environment to develop and sustain thin film of water which reduced the bedrock friction. The additional mass from snow accumulation from the latest storm might have provided the final trigger leading to the devastating ice–rock avalanche on 7 February 2021. Bringing together all the information generated in the study, we propose the possible geometry and process (Mehta et al. 2021), which led to the detachment of the right lobe of the hanging glacier (Fig. 12). The process is related to glacier headwall erosion and matches closely with the modelling result of glacial erosion focusing on abrasion and plucking (Fig. 12C) (MacGregor et al. 2009). It is to be noted that the spatial and temporal scale of the model varies significantly. However, it gives a good understanding of the processes and highlights the need for such modelling effort in the region for small glaciers. This process of headwall erosion is exacerbated by the recent warming of the ground surface, frost cracking, and permafrost thaw and facilitated by increased water availability in the form of increased summer monsoon precipitation and reduction in early winter snow cover. We also propose that the glacier probably gained mass at the accumulation zone owing to the increased summer snowfall. Small glaciers are more susceptible to climate fluctuations and respond faster to the changes. This has been illustrated by recent studies in the region, which suggested small glaciers are losing more mass than big glaciers in recent times (Bhambri et al. 2012; Mir et al. 2017; Yadav et al. 2020). This event highlighted the need for improved monitoring of Himalayan cryospheric systems as complex interlinking snow, glacier, permafrost, geology, and climate cause such catastrophic events.
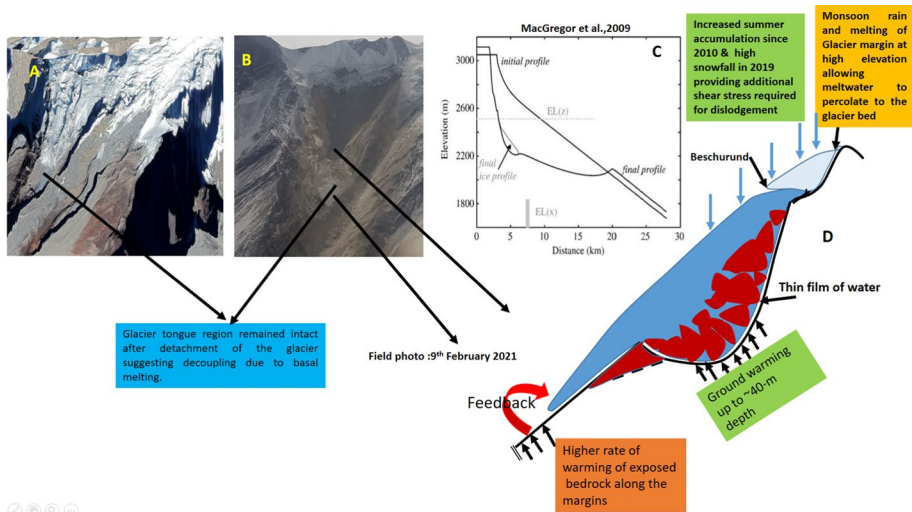
Fig. 12 Schematic sketch of hanging glacier geometry and possible detachment process

5.2 Post-event analysis of stream morphology

After the ice-rock avalanche of the Raunthi hanging glacier, it is suggested that the glacier has melted under frictional heat as it accumulated snow, soil, and rocks on its way downstream and eventually turned into debris flow as it approached the Rishiganga confluence. Further data and studies are required to rebuild the sequence of events unfolded and establish its scientific basis. What certain today is the ice avalanche by a hanging glacier and resultant flood. Snow and soil moisture could add to the floodwaters. A detailed study is required to see if there was any other source for flood water. In the absence of clarity on these aspects, we focussed on the analysis of stream morphological changes between pre-event (used ASTER DEM) and post-event (Digital globe https://www.maxar.com/open-data/uttarakhand-flooding) made of high-resolution spectral images. HEC-RAS 5.0.7 was also used to develop the terrain model of the DEM before generating the stream geometry, bank lines, and flow paths. The stream length from the strike point to the bridge is 13.72 km. Due to debris flow from the ice-rock avalanche, a significant change in the post-event stream width was found. A comparison was made on the surface area of the stream section for the entire length up to the confluence with Dhauliganga through carefully digitising the pre-event and post-event bank lines. It was found that the cumulative pre-event stream width for 13.72 km long stretch was around 50–100 m with a surface area of 0.697 km^2, whereas the post-event channel width increased about 200–250 m with about sixfold increase in the stream surface area (4.22 km^2). Figure 13 shows the post-event massive scouring after the initiation point at Raunthigad. Figure 13b shows no features indicating flood occurrence from the Trishul glacier area. However, a detailed field investigation is necessary to confirm this finding.

5.3 Flood modelling

Developing flood hydrograph originating from such an event is a challenging job. A number of approximations are required for broad understanding at this early stage. Here, we
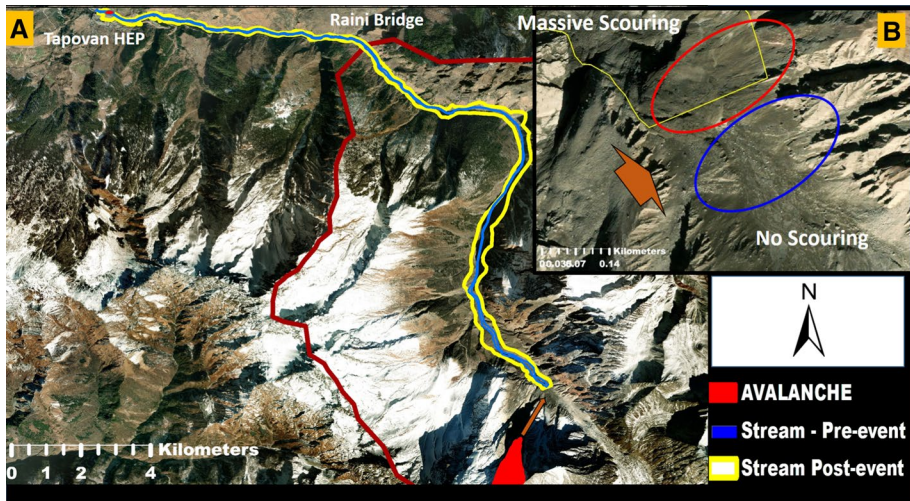
Fig. 13 Images showing **A** pre-event stream width (marked light blue) and post-event scouring (yellow). The location of the hanging glacier and strike point at Raunthigad (marked red) and the stream reach upstream of strike point (marked blue), showing no signs of activities ruling out any flood originating upstream of strike point

used estimated glacier ice volume as the main input. Glacier ice volume estimated as 11.7 to 13.2×10^6 m^3. Additionally, snow and soil moisture from the 3.48 km^2 flood channel area also might have contributed to the final flow volume. As the flood moved downstream in the Raunthigad, it transformed as debris flow by incorporating the scoured material along the river reach. Here we are limiting our estimate to a conservative volume of 10 MCM. The generated hydrograph suggested that the peak flow reaches about 5555 m^3/s within a period of 20–25 min (Fig. S6).

Considering the lack of understanding of the flood generating mechanism at this stage, we consider that the flood acquired its full dimensions about 1 km upstream of the confluence. Taking the generated flood hydrograph as input, we further attempted one-dimensional unsteady flow hydraulic modelling using HEC-RAS 5.0.7 up to the NTPC site located at Tapovan (1800 m a.s.l.). We understand that the flow was supersaturated with debris and ice blocks as learned from local people and could differ with natural streamflow. Specialised debris flow modelling would have been more appropriate under these conditions. The present exercise will provide us with the likely inundation caused due to such a massive flow (~10 MCM), which can be compared with the post-satellite images capturing the inundation.

The HEC-RAS model is set up to simulate flow along the part of the Raunthigad, Rishiganga, and Dhauliganga. The model result of flow depth, velocity, and maximum water spread elevation is shown in Fig. 14. The modelled flood covers the flood channel in a good measure across the channel reach, as seen in the post-event satellite image. The maximum flow depth and velocity simulated utilising the design hydrograph at prominent sections are presented in Table 2. The modelled maximum flow depth and flow velocity reached 33 m and 27 m/s at some cross sections during simulation, indicating the catastrophic nature of the flood. The flow depth and flow velocity at the bridge location were estimated to be 24 m and 12 m/s, respectively. This bridge is completely washed away during the event.
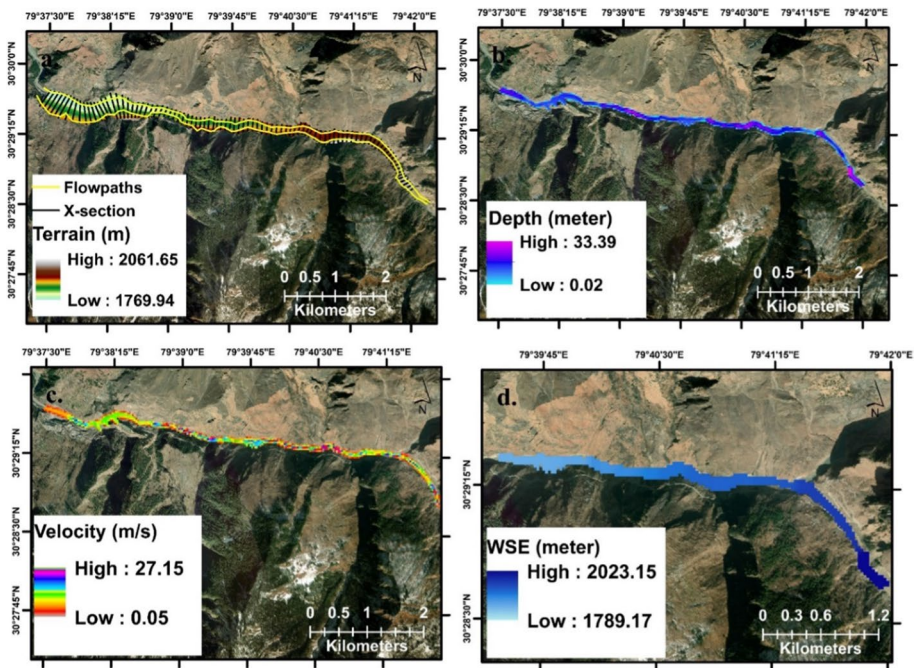
Fig. 14 HEC-RAS model set-up to simulate flow along the cross section up to Tapovan hydropower site

Table 2 Maximum flow depth and probable maximum velocity at locations where the flood damaged the structures

Channel sections	Flow depth (m)	Flow velocity (m/s)
HEP-1	19.7	7.3
BRO Bridge	24.2	12.7
HEP-2	17.7	8.5

The intensity of flow gradually diminished and reached about 8 m/s at HEP 2 at Tapovan. The estimated flow depth at HEP 2 is 17 m. Pandey et al. (2021) estimated the mean modelled depth of debris mixed with water up to 16.3 ± 6.5 m, while the mean modelled velocity of debris along the channel was 22.4 ± 8.6 m/s. This analysis provides a first-order estimate of the flood volume without considering entrained debris with the flow. Better dimensions and strength of the debris flow can be modelled separately.

5.4 Summary observations

- The event is caused by a complex process involving local geology, snow, glacier, permafrost processes, and recent warming of the local climate.
- Regular monitoring of glacier change would have helped to identify the earlier advancement and eventual detachment of the central lobe of this hanging glacier in 2016 and could have served as an early warning.

- Such precursors are common in the Alps and other mountain regions, suggesting an early warning and preparedness is possible in such conditions.
- This event highlighted the vulnerability of the Himalayan cryospheric system to the present warming. System response is building over a period of time due to increased summer precipitation, elevation-depended snow cover change, warming of land surface exacerbated by the seasonal response of reduced snow cover. Delayed response of deeper ground to surface warming, mass balance fluctuations due to increase in summer precipitation, etc. This added a new disaster component in the Himalaya, warranting its regular monitoring at least in the area surrounding infrastructure or development projects, including tourism areas.
- Monitoring the change in precipitation and its form in the high elevation cryospheric areas of the Himalaya is critical for assessing the climate change-related glacier responses. Elevation-depended snow cover change produces a warmer environment surrounding the glacier terminus.
- The response of small glaciers needs regular monitoring as it is more susceptible to changing climate as it responds faster. Also regular monitoring of similar type of glaciers, if any in the region, is required to avoid such type of disasters in future.
- Permafrost studies, including monitoring of ground surface temperature (GST) and modelling of the ground thermal regime, will provide an early indicator. Permafrost elevations in this area and most of the Indian Himalayan region are not known, which will further aggravate the risk of the high elevation cryosphere region under a warming climate.

Declarations

Conflict of interest The authors have no conflicts of interest to declare that are relevant to the content of this article.

References

Allen SK, Rastner P, Arora M, Huggel C, Stoffel M (2016) Lake outburst and debris flow disaster at Kedarnath, June 2013: Hydrometeorological triggering and topographic predisposition. Landslides 13:1479–1491. https://doi.org/10.1007/s10346-015-0584-3

Alley RB, Strasser JC, Lawson DE, Evenson EB, Larson GJ (1999) Glaciological and geological implications of basal-ice accretion in overdeepenings. In: Mickelson DM, Attig JW (eds) Glacial Processes Past and Present. Geological Society of America

Asian News International (7 February 2021) 100–150 casualties feared in the flash flood in Chamoli district: Uttarakhand Chief Secretary OM Prakash to ANI. https://twitter.com/ani/status/1358325017478537217

Awasthi S, Varade D (2021) Recent advances in the remote sensing of alpine snow: A review. Gisci Remote Sens. https://doi.org/10.1080/15481603.2021.1946938

Bhambri R, Bolch T, Chaujar, (2012) Frontal recession of Gangotri Glacier, Garhwal Himalayas, from 1965 to 2006, measured through high-resolution remote sensing data. Curr Sci 102:489–494. https://doi.org/10.5167/uzh-59630

Bahr DB, Meier MF, Peckham SD (1997) The physical basis of glacier volume-area scaling. J Geophys Res 102(B9):20355–20362. https://doi.org/10.1029/97JB01696

Bookhagen B, Burbank D (2006) Topography, Relief, and TRMM-derived rainfall variations along the Himalaya. Geophys Res Lett. https://doi.org/10.1029/2006GL026944

Bookhagen B, Burbank DW (2010) Toward a complete Himalayan hydrological budget: Spatiotemporal distribution of snowmelt and rainfall and their impact on river discharge. J Geophys Res 115:39. https://doi.org/10.1029/2009JF001426

Changwei X, Gough WA, Lin Z, Tonghua W, Wenhui L (2015) Temperature-dependent adjustments of the permafrost thermal profiles on the Qinghai-Tibet Plateau, China. Arct Antarct Alp Res 47:719–728. https://doi.org/10.1657/AAAR00C-13-128

Cheng G, Wu T (2007) Responses of permafrost to climate change and their environmental significance. Qinghai-Tibet Plateau J Geophys Res 112:169. https://doi.org/10.1029/2006JF000631

Cuffey K, Paterson WSBPog (2010) The physics of glaciers, 4th edn. Academic Press, Place of publication not identified

Das S, Ashrit R, Moncrieff M (2006) Simulation of Himalayan cloudburst event. J Earth Syst Sci 115:299–313. https://doi.org/10.1007/BF02702044

Dimri AP, Chevuturi A, Niyogi D, Thayyen RJ, Ray K, Tripathi SN, Pandey AK, Mohanty UC (2017) Cloudbursts in Indian Himalayas: A review. Earth Sci Rev 168:1–23. https://doi.org/10.1016/j.earscirev.2017.03.006

Dobhal D, Mehta M, Srivastava D (2013) Influence of debris cover on terminus retreat and mass changes of Chorabari Glacier, Garhwal region, central Himalaya, India. J Glaciol 59:961–971. https://doi.org/10.3189/2013JoG12J180

Dwivedi S, Neupane Y (2013) Cause and mechanism of the Seti River flood, 5th May 2012, western Nepal. J Nepal Geol Soc. https://doi.org/10.3126/jngs.v46i0.31576

Endrizzi S, Gruber S, DallAmico M, Rigon R (2014) GEOtop 2.0: Simulating the combined energy and water balance at and below the land surface accounting for soil freezing, snow cover and terrain effects. Geosci Model Dev 7:2831–2857. https://doi.org/10.5194/gmd-7-2831-2014

Evans SG, Delaney KB (2015) Catastrophic Mass Flows in the Mountain Glacial Environment. . In: Snow and ice-related hazards, risks, and disasters. pp 563-606. Academic Press

Evans SG, Tutubalina OV, Drobyshev VN, Chernomorets SS, McDougall S, Petrakov DA, Hungr O (2009) Catastrophic detachment and high-velocity long-runout flow of Kolka Glacier, Caucasus Mountains, Russia in 2002. Geomorphology 105:314–321. https://doi.org/10.1016/j.geomorph.2008.10.008

Evans SG, Ge S (2017) Contrasting hydrogeologic responses to warming in permafrost and seasonally frozen ground hillslopes. Geophys Res Lett 50:6788. https://doi.org/10.1002/2016GL072009

Fischer L, Kääb A, Huggel C, Noetzli J (2006) Geology, glacier retreat and permafrost degradation as controlling factors of slope instabilities in a high-mountain rock wall: The Monte Rosa east face. Nat Hazards Earth Syst Sci 6:761–772. https://doi.org/10.5194/nhess-6-761-2006

Govindha Raj KB, Vinod Kumar K (2012) Assessment of supraglacial lake growth from multi-temporal satellite data –A case study of Vasundhara Tal, Kumuon Himalaya, India. Himalayan Geol 33:53–58
    Gubler S, Endrizzi S, Gruber S, Purves R (2013) Sensitivities and uncertainties of modeled ground temperatures in mountain environments. Geosci Model Dev. https://doi.org/10.5194/gmd-6-1319-2013

Haeberli W, Huggel C, Kääb A, Zgraggen-Oswald S, Polkvoj A, Galushkin I, Zotikov I, Osokin N (2004) The Kolka-Karmadon rock/ice slide of 20 September 2002: an extraordinary event of historical dimensions in North Ossetia, Russian Caucasus. J Glaciol 50:533–546. https://doi.org/10.3189/172756504781829710

Hanisch J, Koirala A, Bhandary NP (2013) The Pokhara May 5th flood disaster: a last warning sign sent by nature? J Nepal Geol Soc. https://doi.org/10.3126/jngs.v46i0.31568

Hooke RL (1991) Positive feedbacks associated with erosion of glacial cirques and overdeepenings. Geol Soc Am Bull 103:1104–1108. https://doi.org/10.1130/0016-7606(1991)103%3c1104:PFAWEO%3e2.3.CO;2

Huffman GJ, Bolvin DT, Braithwaite D, Hsu K-L, Joyce RJ, Kidd C, Nelkin EJ, Sorooshian S, Stocker EF, Tan J, Wolff DB, Xie P (2020) Integrated Multi-satellite Retrievals for the Global Precipitation Measurement (GPM) Mission (IMERG). In: Levizzani V, Kidd C, Kirschbaum DB, Kummerow CD, Nakamura K, Turk FJ (eds) Satellite Precipitation Measurement, vol 1. Springer International Publishing, Cham, pp 343–353

Huggel C, Zgraggen-Oswald S, Haeberli W, Kääb A, Polkvoj A, Galushkin I, Evans SG (2005) The 2002 rock/ice avalanche at Kolka/Karmadon, Russian Caucasus: Assessment of extraordinary avalanche formation and mobility, and application of QuickBird satellite imagery. Nat Hazards Earth Syst Sci 5:173–187. https://doi.org/10.5194/nhess-5-173-2005

Huggel C, Allen S, Deline P, Fischer L, Noetzli J, Ravanel L (2012) Ice thawing, mountains falling—are alpine rock slope failures increasing? Geol Today. https://doi.org/10.1111/j.1365-2451.2012.00836.x

Jeng R (2006) NRCS (SCS) Synthetic Curvilinear Dimensionless Unit Hydrograph. J Irrig Drain Eng Asce. https://doi.org/10.1061/(ASCE)0733-9437(2006)132:6(627)

Kargel J, Leonard G, Paudel L, Regmi D, Bajracharya S, Fort M, Joshi S, Poudel K, Thapa B, Watanabe T (2014) The 2012 Seti River flood disaster and alpine cryospheric hazards facing Pokhara, Nepal. In: EGU General Assembly Conference Abstracts, p 12448

Kim DE, Seong YB, Choi KH, Yu BY (2017) Role of debris flow on the change of 10Be concentration in rapidly eroding watersheds: A case study on the Seti River, central Nepal. J Mt Sci 14:716–730. https://doi.org/10.1007/s11629-016-4282-y

Komori J, Koike T, Yamanokuchi T, Tshering P (2012) Glacial lake outburst events in the Bhutan Himalayas. Glob Environ Res 16:59–70

Kumar A, Gupta AK, Bhambri R, Verma A, Tiwari SK, Asthana AKL (2018) Assessment and review of hydrometeorological aspects for cloudburst and flash flood events in the third pole region (Indian Himalaya). Polar Sci 18:5–20. https://doi.org/10.1016/j.polar.2018.08.004

MacGregor KR, Anderson RS, Waddington ED (2009) Numerical modeling of glacial erosion and headwall processes in alpine valleys. Geomorphology 103:189–204. https://doi.org/10.1016/j.geomorph.2008.04.022

Mehta M, Kumar V, Sain K, Tiwari S, Kumar A, Verma A (2021) Causes and consequences of rishiganga flash flood, nanda devi biosphere reserve, Central Himalaya, India. Curr Sci 21:1484–1487. https://doi.org/10.18520/cs/v121/i11/1483-1487

Mergili M, Emmer A, JvYicová A, Cochachin A, Fischer J-T, Huggel C, Pudasaini SP (2018) How well can we simulate complex hydro-geomorphic process chains? The 2012 multi-lake outburst flood in the Santa Cruz Valley (Cordillera Blanca, Perú). Earth Surf Proc Land 43:1373–1389

Mergili M, Jaboyedoff M, Pullarello J, Pudasaini SP (2020) Back calculation of the 2017 Piz Cengalo-Bondo landslide cascade with r. avaflow: What we can do and what we can learn. Nat Hazards Earth Syst Sci 20:505–520. https://doi.org/10.5194/nhess-20-505-2020

Mir RA, Jain SK, Jain SK, Thayyen RJ, Saraf AK (2017) Assessment of recent glacier changes and its controlling factors from 1976 to 2011 in Baspa Basin, Western Himalaya. Arct Antarct Alp Res 49:621–647. https://doi.org/10.1657/AAAR0015-070

Mishra PK, Singh H, Renoj J., Das S, Nema MK, Kumar P (eds) (2021): Block level Livelihood Vulnerability Index of a Himalayan district in Upper Ganga Basin

Mishra PK, Thayyen RJ, Singh H, Das S, Nema MK, Kumar P (2022) Assessment of cloudbursts, extreme rainfall and vulnerable regions in the Upper Ganga basin, Uttarakhand, India. Int J Disaster Risk Reduct 69:102744. https://doi.org/10.1016/j.ijdrr.2021.102744

Oi H, Higaki D, Yagi H, Usuki N, Yoshino K (2014) Report of the investigation of the flood disaster that occurred on May 5, 2012 along the Seti River in Nepal. IJECE 7:111–117. https://doi.org/10.13101/ijece.7.111

Pandey P, Chauhan P, Bhatt CM, Thakur P, Kannaujiya S, Dhote PR, Roy A, Kumar S, Chopra S, Aggarwal S, Bhardwaj A (2021) Cause and process mechanism of rockslide triggered flood event in rishiganga and Dhauliganga river valleys, Chamoli, Uttarakhand, India Using Satellite Remote Sensing and in situ Observations. J Indian Soc Remote Sens 49:1011–1024. https://doi.org/10.1007/s12524-021-01360-3

Paterson WSB (1994) The physics of glaciers, 3rd edn. Pergamon, Oxford

Pogliotti P (2011) Influence of snow cover on MAGST over complex morphologies in mountain permafrost regions. Ph.D. Thesis, Università degli Studi di Torino, Torino, Italy

Preh A, Sausgruber JT (2015) The Extraordinary Rock-Snow Avalanche of Alpl, Tyrol, Austria. Is it Possible to Predict the Runout by Means of Single-phase Voellmy- or Coulomb-Type Models? In: Engineering Geology for Society and Territory-Volume 2. pp 1907–1911. Springer, Cham

Rana N, Sharma S, Sundriyal Y, Kaushik S, Pradhan S, Tiwari G, Khan F, Sati SP, Juyal N (2021) A preliminary assessment of the 7th February 2021 flashflood in lower Dhauli Ganga valley, Central Himalaya. India J Earth Syst Sci 130:50. https://doi.org/10.1007/s12040-021-01608-z

Röthlisberger H (1987) Sliding phenomena in a steep section of Balmhorngletscher Switzerland. J Geophys Res 92:8999. https://doi.org/10.1029/JB092iB09p08999

Sangewar CV, Shukla SP, Singh RK, Geological Survey of India (2009) Inventory of the Himalayan glaciers: A contribution to the international hydrological programme (Updated ed.), 7th edn. APA (7th ed.), Calcutta, India

Savi S, Comiti F, Strecker MR (2021) Pronounced increase in slope instability linked to global warming: A case study from the eastern European Alps. Earth Surf Process Landforms 46:1328–1347. https://doi.org/10.1002/esp.5100

Schmidt S, Nüsser M, Baghel R, Dame J (2020) Cryosphere hazards in Ladakh: The 2014 Gya glacial lake outburst flood and its implications for risk assessment. Nat Hazards. https://doi.org/10.1007/s11069-020-04262-8

Service E (2007) National Engineering Handbook, US. SERBIULA (sistema Librum 2.0) sec. 4

Shukla D, Dubey C, Ningreichon A, Usham A (2013) Orographic control of the Kedarnath disaster. Curr Sci 105:1474–1476

Singh M, Thayyen R, Jain S (2019) Snow cover change assessment in the upper Bhagirathi basin using an enhanced cloud removal algorithm. Geocarto Int. https://doi.org/10.1080/10106049.2019.1704069

Thakur VC (1992) Geology of western Himalaya. Phys Chem Earth 19:1–355

Thayyen R, Dimri AP (2018) Slope environmental lapse rate (SELR) of temperature in the monsoon regime of the Western Himalaya. Front Environ Sci 6:42. https://doi.org/10.3389/fenvs.2018.00042

Thayyen R, Gergan JT, Dobhal D (2005) Lapse rate of slope air temperature in a Himalayan catchment - a study from Din Gad (Dokriani Glacier) basin, Garhwal Himalaya. India Bull Glaciol Res 22:19–25

Thayyen R, Dimri AP, Kumar P, Agnihotri P (2013) Study of cloudburst and flash floods around Leh, India during August 4–6, 2010. Nat Hazards 65:2175–2204. https://doi.org/10.1007/s11069-012-0464-2

Thayyen RJ (2020) Hydrology of the Cold-Arid Himalaya: Himalayan Weather and Climate and their Impact on the Environment, 2020. Springer International Publishing

Thayyen RJ, N Kumar, Goel MK, Kotwal SP (2010) Estimation of aerial and volumetric changes of selected glaciers in Jammu & Kashmir. http://117.252.14.250:8080/jspui/handle/123456789/6045

Varade D, Dikshit O (2018) Assessment of Winter Season Land Surface Temperature in the Himalayan regions around the Kullu area in India using Landsat-8 data. Geocarto Int. https://doi.org/10.1080/10106049.2018.1520928

Wani JM, Thayyen RJ, Gruber S, Ojha CSP, Stumm D (2020) Single-year thermal regime and inferred permafrost occurrence in the upper Ganglass catchment of the cold-arid Himalaya, Ladakh. India Sci Total Environ 703:134631. https://doi.org/10.1016/j.scitotenv.2019.134631

Wegmann M, Gudmundsson G, Haeberli W (1998) Permafrost changes in rock walls and the retreat of alpine glaciers: A thermal modelling approach. Permafr Periglac Process 9:23–33. https://doi.org/10.1002/(SICI)1099-1530(199801/03)9:1<23.0.CO;2-Y

Wu Q, Zhang T (2008) Recent permafrost warming on the Qinghai-Tibetan Plateau. J Geophys Res 113:99. https://doi.org/10.1029/2007JD009539

Yadav BC, Thayyen RJ, Jain K (2020) Topoclimatic zones and characteristics of the upper Ganga basin, Uttarakhand, India. Int J Climatol 40:6002–6019. https://doi.org/10.1002/joc.6562

Authors and Affiliations

**Renoj J. Thayyen[1] · P. K. Mishra[1] ⓘ · Sanjay K. Jain[1] · John Mohd Wani[1] ·
Hemant Singh[1,2] · Mritunjay K. Singh[1,3] · Bankim Yadav[4]**

✉ P. K. Mishra
   erprabhash@gmail.com

1   National Institute of Hydrology, WRS Division, Roorkee 247667, India

2   Department of Civil Engineering, Indian Institute of Technology, Jammu 181221, India

3   National Space Science and Technology Center (NSSTC), UAE University, P.O Box. 15551,
    Al Ain, UAE

4   Indian Institute of Technology Roorkee, Roorkee 247669, India